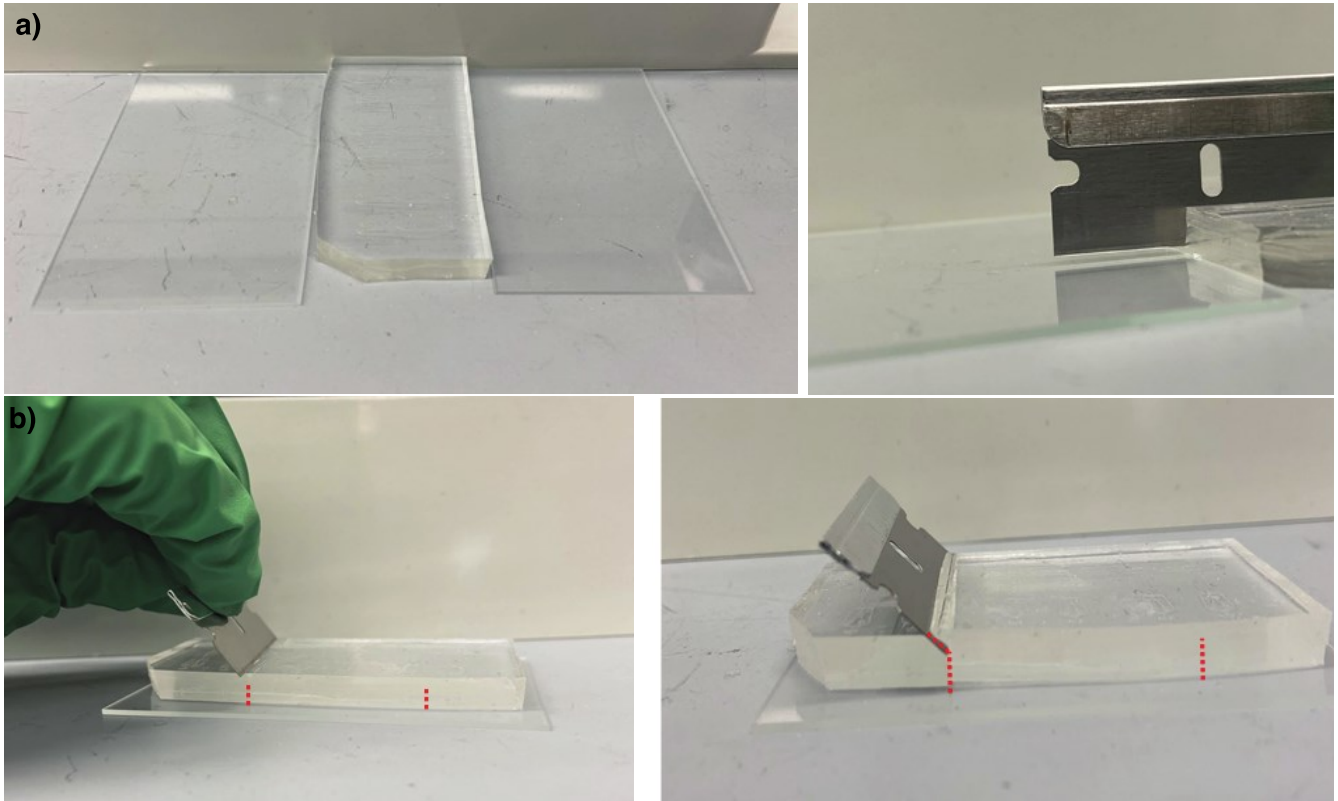
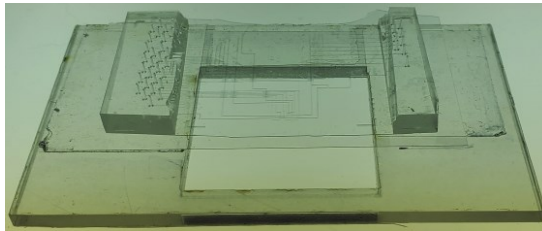
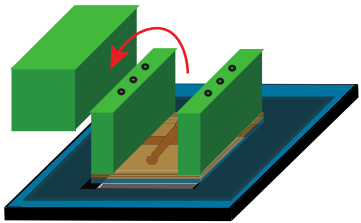
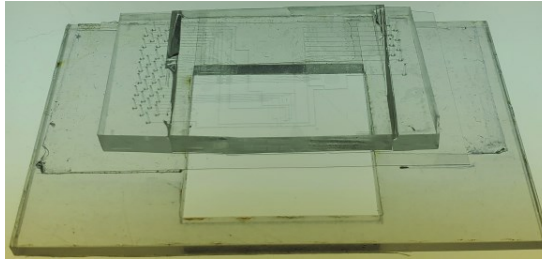
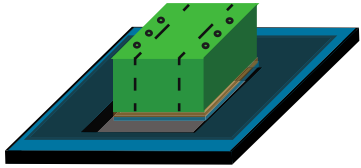


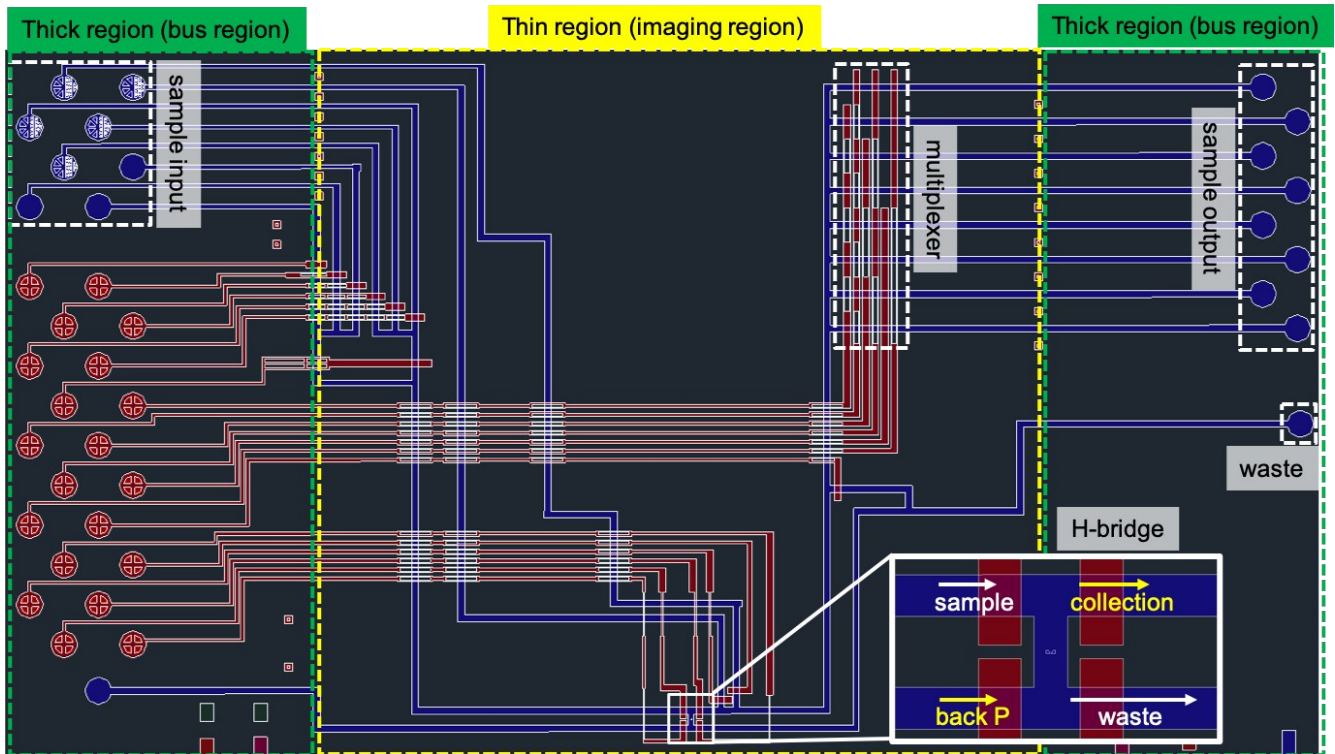
Supplementary Information



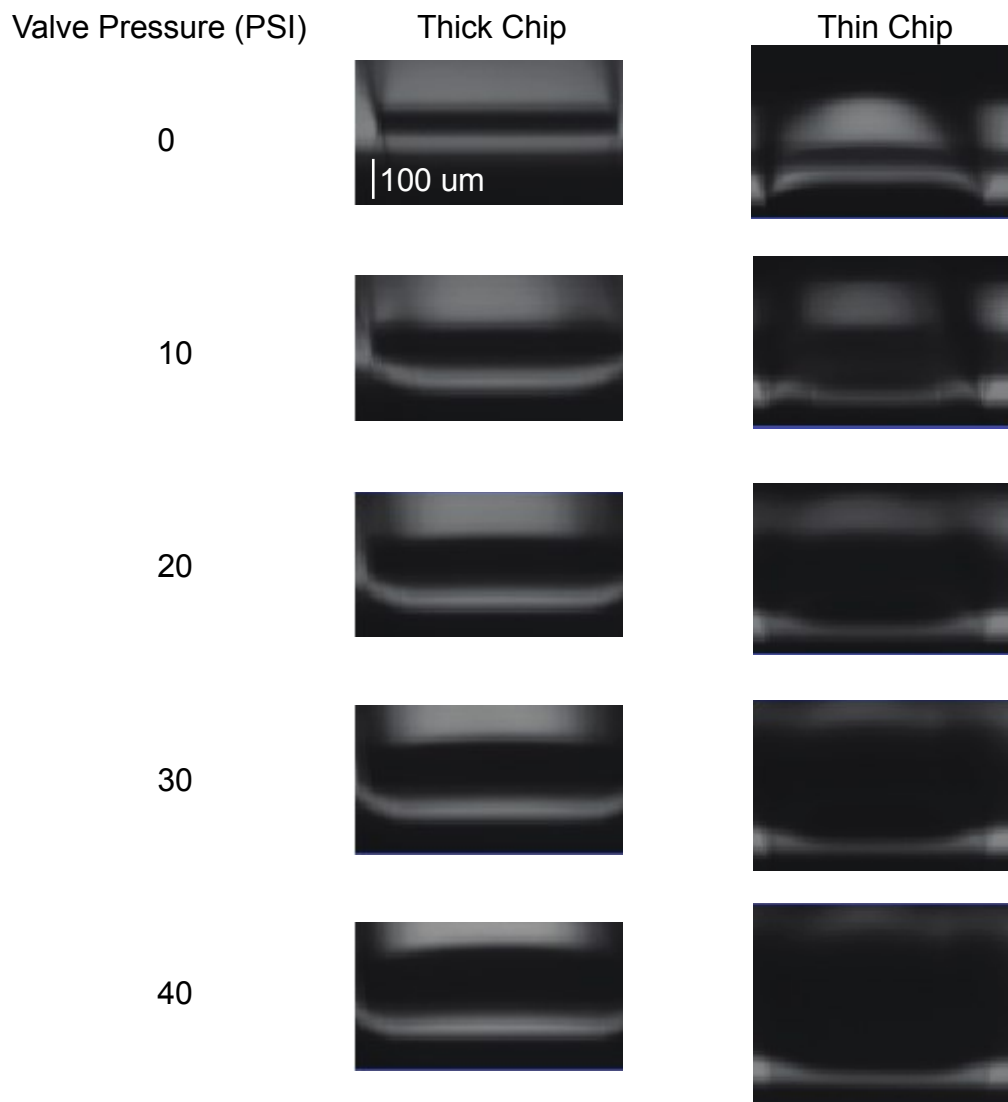
Supplementary figure 1. a) Carrier pre-cutting process. Glass slides used as stoppers to prevent the razor blade from cutting the PDMS all the way through, leaving a 1mm gap on what will be the top side on the fully assembled device. **b)** Carrier final cut. After assembly of the 4 layer device (from bottom to top: glass - flow - control - carrier), the final cuts are made for the removal of the center portion of the carrier layer to reveal the imaging window. Using a razor blade, a 45 degree angled cut is made from the top until it reaches the pre-cut section. After both sides are cut in this manner, the center portion of the carrier layer is fully through-cut and can be carefully peeled off.



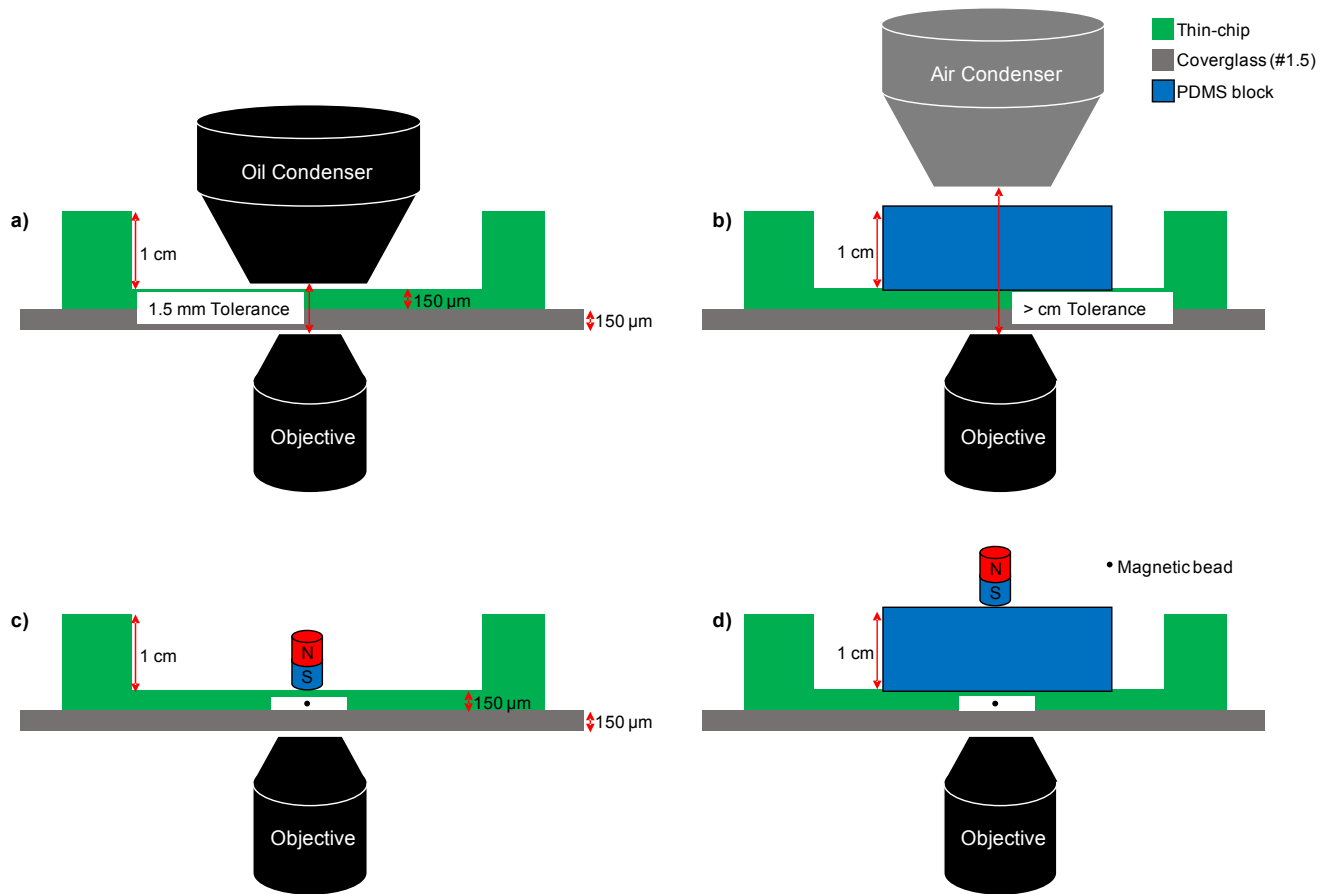
Supplementary figure 2. Schematic (left) and photo (right) of the thin-chip mounted on the adapter. The adapter (top) is mounted with the thin-chip on a number 1.5 cover-glass (middle), where the middle part of the carrier is peeled away to expose the thin imaging region (bottom).



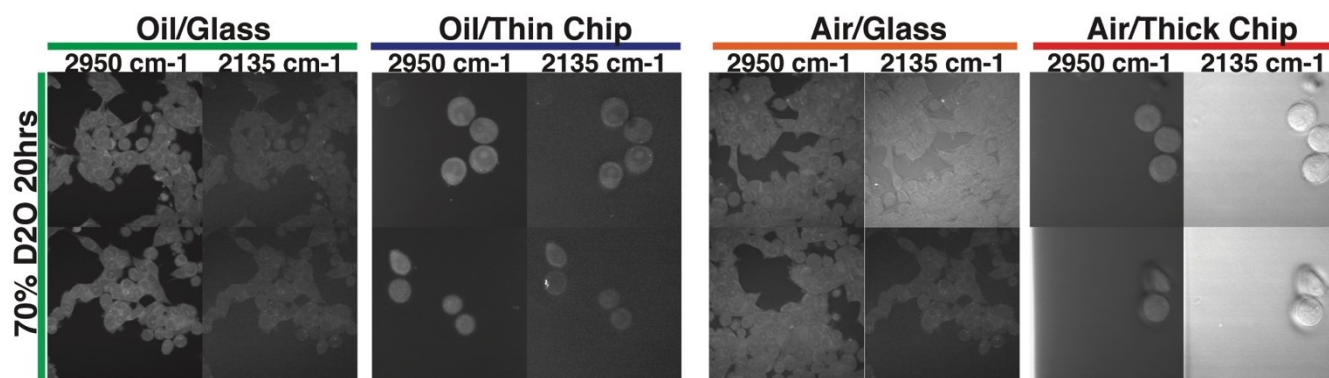
Supplementary figure 3. The CAD design of the thin single-cell sorting chip. The chip has sample inputs and outputs, an H-bridge cell imaging area and sorter, and a multiplexer (white dotted boxes). The middle area is the imaging region (yellow dotted box) flanked on both sides by the thick bus region (green dotted box).



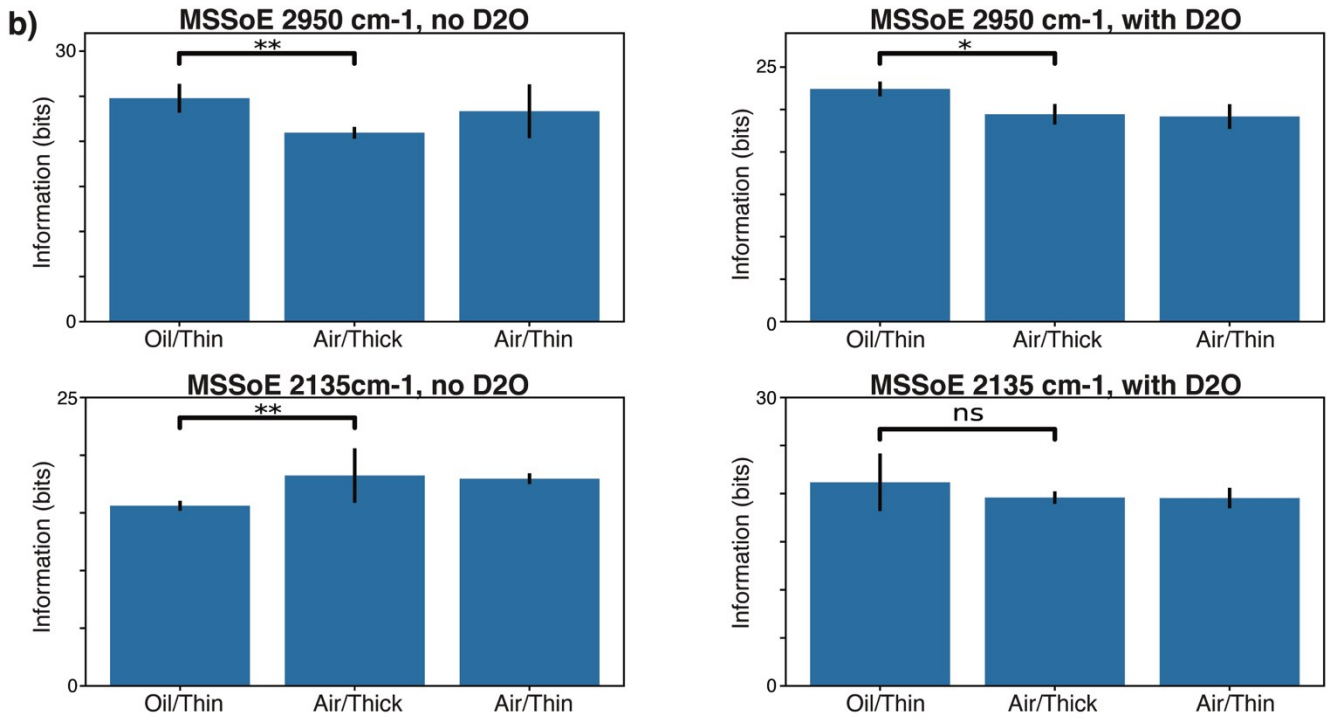
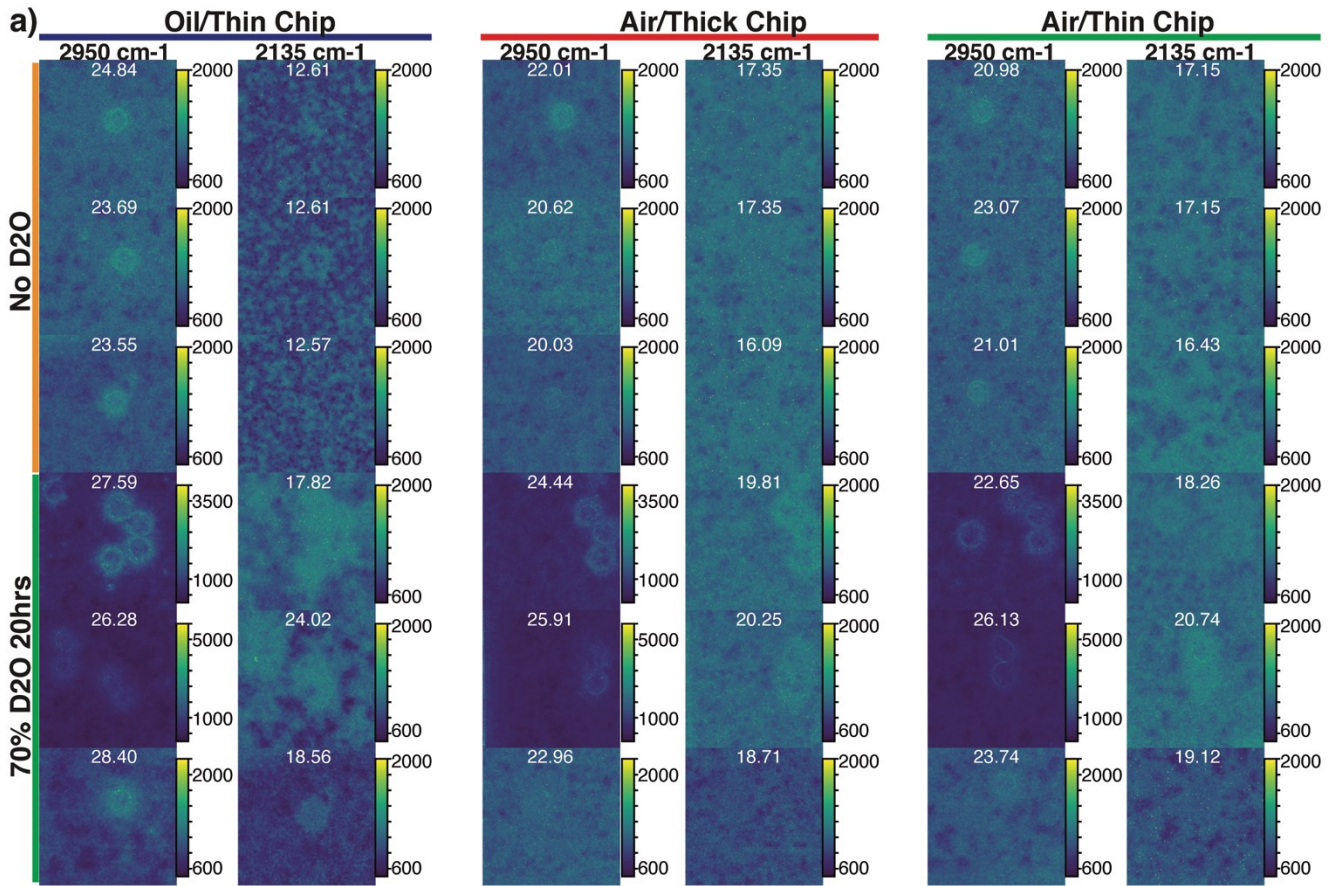
Supplementary figure 4. Micro-valve deformation comparison between the thin and thick chip. The vertical cross-section of the micro-valve is obtained by scanning the SRS microscope in xz while gradually increasing the valving pressure.



Supplementary figure 5. The schematic of the experimental configuration for the thin-chip and thick chip mimic on the inverted microscope. The configuration for SRS cell imaging on the **a)** thin-chip with an oil condenser and **b)** the thick chip mimic with an air condenser. The experimental setup for the magnetic bead manipulation experiment on **c)** the thin-chip and **d)** the thick chip mimic. The components, size, and distances are labeled (not to scale).



Supplementary figure 6. Single cell SRS imaging on coverglass was performed to compare against images acquired using the thin- and thick chip with both the air and oil immersion condensers.



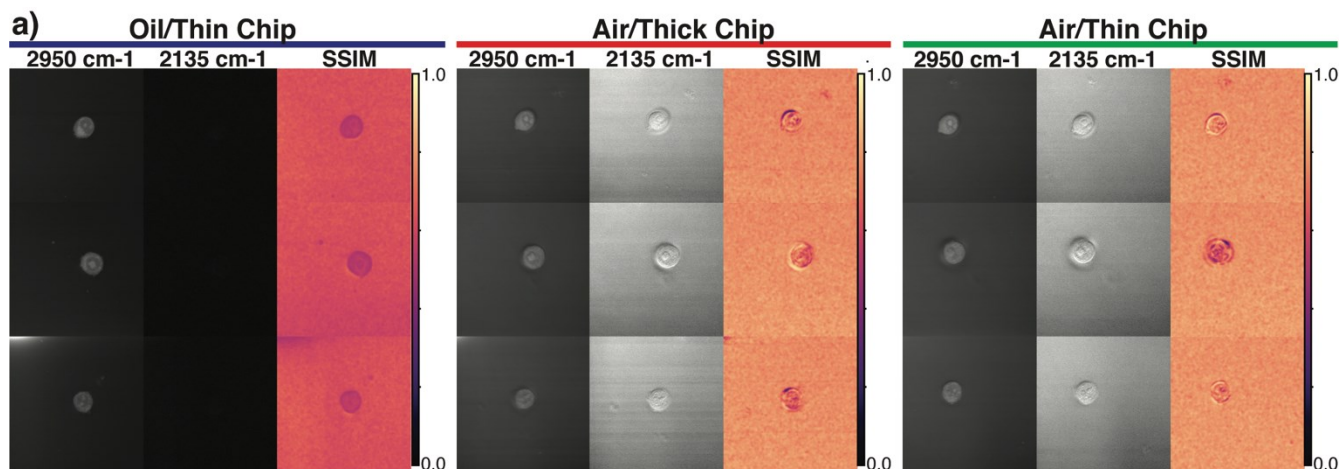
Supplementary figure 7. Multi-scale Second order Entropy (MSSoE). a) MSSoE maps for cells not presented in figure 3c. Note scaling, and cut-offs, are arbitrary and are intended solely to highlight which features contributed most strongly to the actual overall MSSoE. Yellow/green indicates greater contribution to the score. b) Comparison of the overall MSSoE across the 3 imaging conditions for the

no D2O (left) and D2O (right) samples, in the 2950 cm^{-1} (top) and 2135 cm^{-1} (bottom) channels. Note that while the difference between the oil/thin and air/thick conditions in the 2135 cm^{-1} channel for D2O containing cells is not significant, this is not surprising. The contribution from XPM in the thick/air condition provides a contrast mechanism which generates information in the image; however, it is non-specific and not the desired Raman signal.

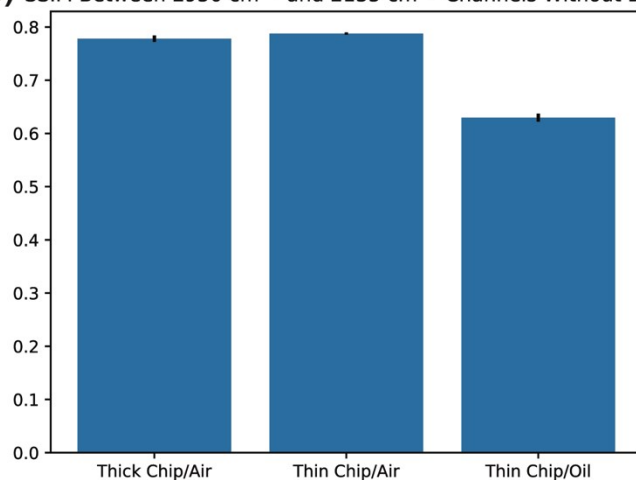
** : One-sided Mann-Whitney $U = 0$, $n = 5$, significance level = 0.005

* : One-sided Mann-Whitney $U = 0$, $n = 3$, significance level = 0.05

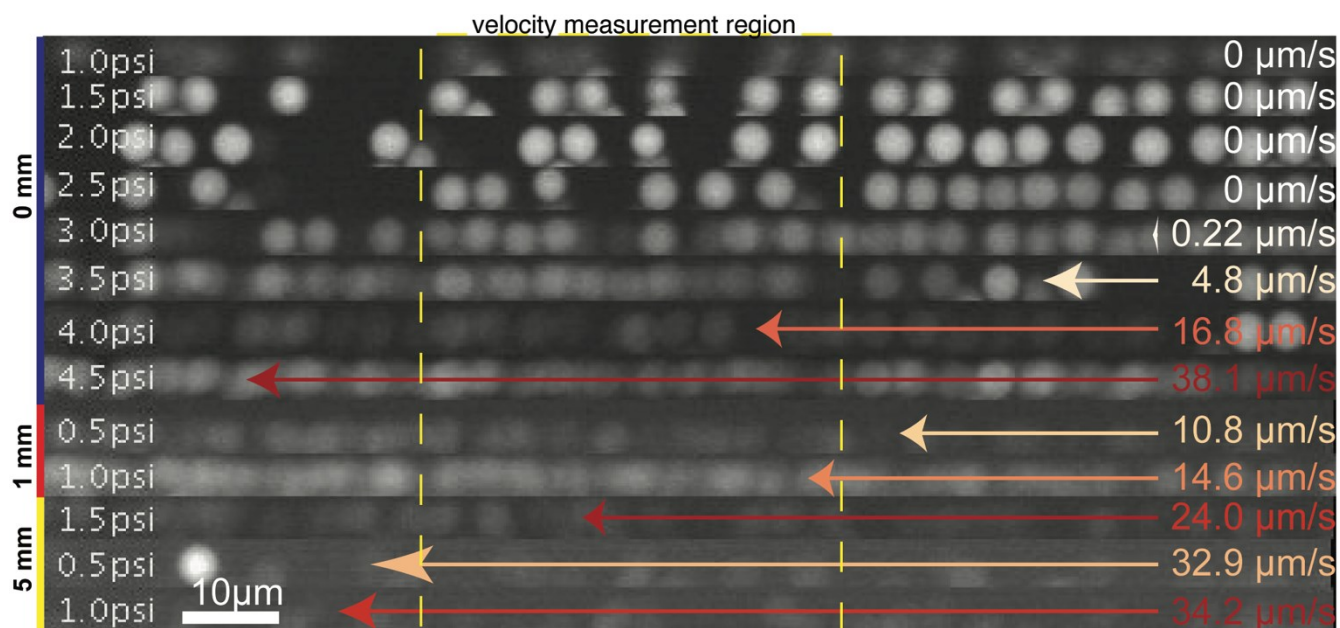
ns: Not Significant



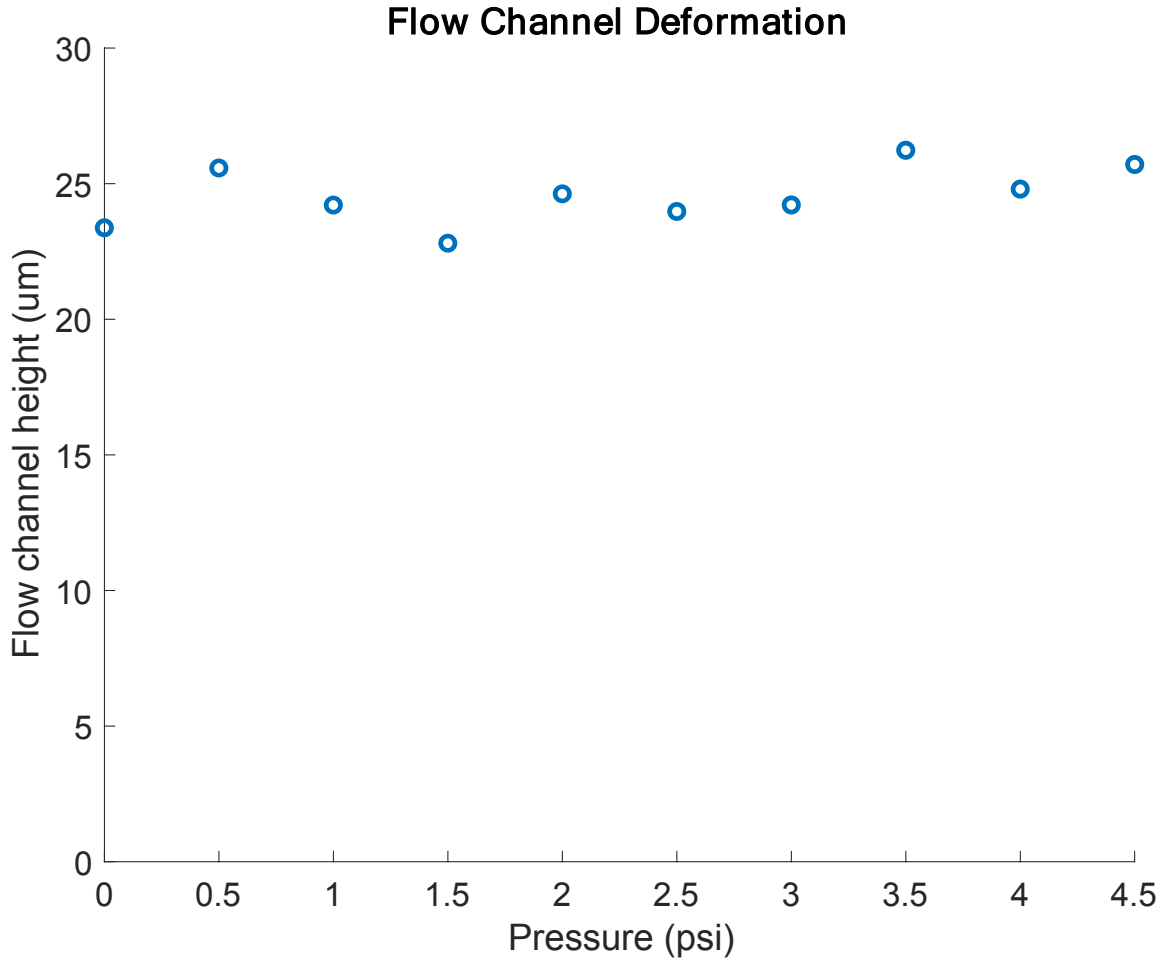
b) SSIM Between 2950 cm⁻¹ and 2135 cm⁻¹ Channels Without D₂O



Supplementary figure 8. SSIM a) SSIM images for cells not presented in figure 3d. The Scale is renormalized from 0 to 1. Only non-D₂O cells are compared as the ground truth for similarity, if any, between the 2135 cm⁻¹ and 2950 cm⁻¹ channels for cells incubated with D₂O is unknown. b) Mean SSIM and standard deviation for all non-D₂O cells across the three imaging conditions.



Supplementary figure 9. The magnetic bead controllability in the flow channel of a valve-microfluidic device, measured at varying magnet distance and flow pressure. The velocity of 3 μm fluorescent magnetic beads was measured in the flow channel of the thin-chip. The flow pressure and distance between the magnet and the top surface of the thin-chip is indicated on the left, where the magnet placed directly on top is 0 mm (blue). The bead velocity was measured in the velocity measurement region (yellow dotted line). The mean velocity of $n = 5$ is shown on the right with the arrow length and color denoting the magnitude ($\mu\text{m/s}$). All frames of the video were super-imposed into one single image to show motion, where distinct bead edges indicate still beads while motion is indicated by blurring. The full video is available as supplementary video 1. The beads were imaged via two-photon excited fluorescence at a wavelength of 900 nm, with an excitation power of 20 mW, and a pixel dwell time of 2 μs . The scale bar on the bottom left indicates 10 μm .



Supplementary figure 10. The flow channel deformation was measured at varying flow pressures. This was measured by filling the flow channel with D2O and z-scanning the center of the flow channel collecting the SRS signal of the D2O molecules. With Hagen-Poiseuille's standard flow kinetic equation,

$$P = \frac{8\mu l Q}{\pi r^4}$$

where:

- P is the pressure drop
- l is the length of the channel
- Q is the volumetric flow rate
- r is the radius of the channel

and

$$Q = Av = \pi r^2 v$$

where:

- v is the flow velocity

we can approximate

$$v \propto Pr^2$$

Thus, since the flow pressure has negligible effect on the flow channel deformation in the thin-chip, we expect the bead velocity to increase linearly with the flow pressure when the bead velocity matches the surround flow.